2009 American Control Conference
Hyatt Regency Riverfront, St. Louis, MO, USA
June 10-12, 2009

Structural Damage Localization with Tolerance to Large Time Synchronization Errors in WSNs

Guirong Yan, Shirley J. Dyke, Wei Song, Gregory Hackmann and Chenyang Lu

Abstract—With recent technological advances in smart sensor platforms, structural condition monitoring implementations based on Wireless Sensor Networks (WSNs) have received considerable attention. Modal identification is an integral step in many structural condition monitoring systems. However, accurate time synchronization is not always possible, leading to incorrect identification of the mode shapes. Although strict time synchronization of the wireless sensors has been viewed as crucial for the identification of mode shapes, a new perspective is taken herein. The distortion in the identified mode shapes is characterized and accommodated. Then the resulting mode shapes are used with a flexibility-based damage detection approach to localize damage to the exact elements. Numerical simulations considering a simply supported beam are used to demonstrate that the requirement of frequent sensor synchronization can be relaxed with this approach, without sacrificing accuracy in the results.

I. Introduction

Recent catastrophic failures of civil infrastructures around the world underscore the need for more reliable and robust structural health monitoring (SHM) systems. With recent technological advances in wireless communication, the SHM system based on Wireless Sensor Network (WSN) has shown considerable promise [1,2,3].

However, a new challenge, time synchronization errors (TSEs) between different wireless sensing units, has been presented in WSNs due to clock imprecision or sensor blockage [4]. To solve this problem, some communication protocols between the central server and the wireless sensing units have been presented, for example, timestamp synchronization [4], reference broadcast synchronization [5], flood time-synchronization protocol [6], etc.. The basic idea of most protocols is to provide a mechanism to synchronize the local clocks of the sensor nodes within the WSN. However, even if these protocols are employed in a WSN, completely synchronized measurement data are not necessarily guaranteed. For instance, for a long-term monitoring system, larger TSEs will be accumulated with time due to the clock drift after one synchronization is performed. Therefore, frequent time resynchronization is required, which results in large energy consumption and large communication bandwidth occupancy. In addition, when sensing is running, time synchronization may not perform well [7].

In many structural condition monitoring systems, modal identification is an integral step. TSEs in WSNs usually distort the identification results of mode shapes, which will prohibit obtaining correct damage detection results. Krishnamurthy et al. [8] studied the influence of the TSE on the identified mode shapes and found that the TSE affected the amplitudes of mode shapes. However, they overlooked the influence on the phase information in these mode shapes.

In this study, we will systematically investigate the influence of the TSE on the identified mode shapes. Then the time synchronization problem will be addressed from a new perspective. Our goal is not time synchronization, but rather to propose damage detection strategies which are tolerant of large TSEs. First, the distorted mode shape is corrected to some extent according to the influence of TSEs on the identification results of mode shapes, and then the resulting mode shapes are applied for damage detection. In this way, the time resynchronization rate may be reduced.

II. System Identification and Damage Detection

A. System identification using the FDD method

Considering that the unmeasurable ambient vibration is usually taken as the external excitation for civil structures, an output-only system identification method, the Frequency Domain Decomposition (FDD) method, is selected to identify structural modal parameters.

The following procedures are used for the FDD method. First, the cross spectral density (CSD) matrix of the response at each discrete frequency point is estimated. For instance, the CSD matrix corresponding to the mth natural frequency is expressed as (assuming that the kth frequency point is associated with the mth natural frequency)

$$\mathbf{G}(\omega_m)=\mathbf{G}(k)=\begin{bmatrix} X_1(k)X_1^*(k) & \cdots & X_1(k)X_i^*(k) & \cdots & X_1(k)X_n^*(k) \\ \vdots & & \vdots & & \vdots \\ X_i(k)X_1^*(k) & \cdots & X_i(k)X_i^*(k) & \cdots & X_i(k)X_n^*(k) \\ \vdots & & \vdots & & \vdots \\ X_n(k)X_1^*(k) & \cdots & X_n(k)X_i^*(k) & \cdots & X_n(k)X_n^*(k) \end{bmatrix} \quad (1)$$

Guirong Yan, a post-doctor, is with the Department of Mechanical, Aerospace, and Structural Engineering (MASE), Washington University, St. Louis, MO 63130 USA. (corresponding author, phone: 314-935-4126, e-mail: yan.g@seas.wustl.edu) and Harbin Institute of Technology in China.

Shirley J. Dyke, a professor, is with the Department of MASE, Washington University, St. Louis, MO 63130 USA. (e-mail: sdyke@seas.wustl.edu).

Wei Song, PhD student, is with the Department of MASE, Washington University, St. Louis, MO 63130 USA. (e-mail: weisong@wustl.edu)

Gregory Hackmann, PhD student, is with Department of Computer Science and Engineering (CSE), Washington University, St. Louis, MO 63130 USA. (e-mail: gwh2@cse.wustl.edu)

Chenyang Lu, an associate professor, is with the Department of CSE, Washington University, St. Louis, MO 63130 USA. (e-mail: lu@cse.wustl.edu)

where $X_i(k)$ reprsents the Discrete Fourier Transform (DFT) of the response $x_i(n)$, and $\bullet^*$ represents the conjugate transpose operation.

Then a Singular Value Decomposition (SVD) is performed on the CSD matrix at each frequency point. The maximum singular value in each singular value matrix is obtained, and all the maximum singular values form a vector. The frequency points corresponding to the peaks of this vector are identified as the natural frequencies. The first column of the left singular decomposition matrix corresponding to one natural frequency is an estimate of this mode shape [9].

Because the mode shapes are only relative to the left singular decomposition matrices, herein the SVD of a CSD matrix can be calculated by means of solving an eigenvalue problem [10]. For instance, for the CSD matrix at $\omega = \omega_m$

$$\mathbf{G}(\omega_m)\mathbf{G}^*(\omega_m) = \mathbf{U}\mathbf{\Sigma}^2\mathbf{U}^* = \mathbf{U}\mathbf{\Sigma}\mathbf{\Sigma}^*\mathbf{U}^* \tag{2}$$

Therefore, let

$$\mathbf{G}(\omega_m) = \mathbf{U}\mathbf{\Sigma} \tag{3}$$

where $\mathbf{\Sigma}$ and $\mathbf{U}$ denote the singular value matrix and the left singular decomposition matrix, respectively. $\mathbf{\Sigma}$ is a diagonal matrix.

Herein the first column of $\mathbf{U}$ is an estimate of the *m*th mode shape and is designated $\mathbf{U}_1$. By dividing all of the components of $\mathbf{U}_1$ by one of the components of $\mathbf{U}_1$ chosen as a reference, the normalized mode shape is obtained. Its components are complex values. The phase of each complex value represents the phase difference between each response and the reference. To get the real-value components of the mode shape, the moduli of $\mathbf{U}_1$ are first calculated to obtain the magnitudes of this mode shape, and their signs are determined by their respective phases. The phases of the components in the normalized mode shape should be 0 or π for linear and proportional-damping systems. If the phase is 0, the corresponding sign is positive; if the phase angle is π, the corresponding sign is negative. Due to the presence of the measurement and identification errors in practice, the phases are not strictly 0 or π. Therefore, the signs of the components are determined in the following way: if the phase is in the range of $[-\pi/2 \quad \pi/2]$, the corresponding sign is positive; otherwise, if the phase is in the range of $[-\pi/2 \quad 3\pi/2]$, the corresponding sign is negative.

A. Damage detection using flexibility-based methods

Flexibility-based methods will be employed here, because the flexibility matrix can be estimated accurately using few lower-frequency modes and the measurement DOFs (Degrees of Freedom) are not required to be complete.

B.1 The classical flexibility difference method

Based on the fact that the presence of damage in structures reduces structural stiffness, and increases structural flexibility, the change in structural flexibility in the pre- and post-damaged states can be used to detect damage. The change in flexibility **F** can be computed as

$$\Delta\mathbf{F} = \mathbf{F}^d - \mathbf{F}^u \tag{4}$$

where the superscripts *d* and *u* indicate the damaged and undamaged structures, respectively. The flexibility can be assembled by modal parameters as

$$\mathbf{F} = \sum_{r=1}^{n} \frac{1}{\omega_r^2}\boldsymbol{\varphi}_r\boldsymbol{\varphi}_r^T \tag{5}$$

where $\boldsymbol{\varphi}_r$ is the *r*th mass-normalized mode shape, ω_r is the *r*th circular modal frequency, and *n* is the number of modes used. The diagonal entries or the maximum absolute values of the elements in each column of $\Delta\mathbf{F}$ are extracted to form a vector, from which the damage location can be found [11].

B.2 ASH flexibility-based method

Because the damage detection results using classical flexibilities are embodied as nodal or DOF's characterization, the classical flexibility difference method cannot directly localize damage to the exact elements. Herein the ASH flexibility-based method (ASHF method for short) will be employed for detecting damage in beam-like structures. This method measures the change in Angles-between- String-and-Horizon (ASH) of beam elements caused by damage and thus it can localize damage to the exact elements. The other advantages of this method over the classical flexibility-based damage detection methods are referred to [12].

The ASH flexibility matrix can be constructed as

$$\mathbf{F}_\theta = \sum_{r=1}^{n} \frac{1}{\omega_r^2}\mathbf{R}_r\mathbf{R}_r^T \tag{6}$$

where $\mathbf{R}_r$ is called the *r*th ASH mode shape, and it can be expressed in terms of the *r*th translational mode shape as

$$\mathbf{R}_r = \left[\frac{1}{l_1}\varphi_{1,r} \quad \frac{1}{l_2}(\varphi_{2,r}-\varphi_{1,r}) \quad \cdots \quad \frac{1}{l_i}(\varphi_{i,r}-\varphi_{i-1,r}) \quad \cdots \quad \frac{1}{l_n}(\varphi_{n,r}-\varphi_{n-1,r})\right]^{\mathrm{T}} \tag{7}$$

The elements in the *r*th column of this flexibility matrix represent the ASHs of all elements of the beam resulting from a unit moment applied at two nodes of element *r* of the beam, and no force or moment on the other elements. The element in the ASH flexibility is associated with a beam-element rather than a node.

The diagonal or the maximum absolute values of the elements in each column in the difference of ASH flexibility matrices between the pre- and post-damaged structures are extracted as damage indicators of elements. By observing the "step and jump" in the plot of damage indicators vs. numbers of elements, the damage sites in structures can be determined.

III. THE INFLUENCE OF NON-SYNCHRONIZED SENSING ON IDENTIFICATION RESULTS OF MODE SHAPES AND CORRECTION

In this section, the effect of the TSEs on the identified mode shapes is first investigated, and then a strategy for adjusting the resulting distorted mode shapes is proposed.

Considering the TSE between wireless sensors, the response measured from the *i*th sensor is expressed as

$$\tilde{x}_i(t) = x_i(t + \delta t_i) \tag{8}$$

where δt_i is the TSE between the *i*th wireless sensor and the time reference sensor. Its Fourier transform is obtained as

$$\tilde{X}_i(\omega) = \mathbf{F}\left[\tilde{x}_i(t)\right] = \mathbf{F}\left[x_i(t+\delta t_i)\right] = e^{i\omega\delta t_i} X_i(\omega) \quad (9)$$

where $\mathbf{F}[\bullet]$ represents the operator, and $X_i(\omega)$ is the Fourier Transform of $x_i(t)$.

Equations (8) and (9) are for the continuous Fourier Transform under ideal conditions. In practice,the DFT is used and thus we need to explore the relationship between the DFTs of the data with and without a TSE. Consider one set of digital data $x(n)$ as the data without the TSE and $\tilde{x}(n)$ as the data with the TSE. They are expressed as

$$\begin{aligned} x(n) &= \left[x(1) \quad x(2) \quad \cdots \quad x(N-1) \quad x(N)\right] \\ \tilde{x}(n) &= \left[x(3) \quad x(4) \quad \cdots \quad x(N+1) \quad x(N+2)\right] \end{aligned} \quad (10)$$

The DFTs of $x(n)$ and $\tilde{x}(n)$ can be expressed as

$$X(k) = \sum_{n=1}^{N} x(n) e^{-j\frac{2\pi(n-1)k}{N}} \quad (11)$$

$$\tilde{X}(k) = \sum_{n=1}^{N} \tilde{x}(n) e^{-j\frac{2\pi(n-1)k}{N}} \quad (12)$$

The two sides of Eq. (12) are multiplied by $e^{-j\frac{2\pi\bullet 2\bullet k}{N}}$ and subtracted from Eq. (11), yielding

$$\tilde{X}(k) = \left(X(k) + (x(N+1) - x(1)) e^{-j\frac{2\pi\bullet 0\bullet k}{N}} + (x(N+2) - x(2)) e^{-j\frac{2\pi\bullet 1\bullet k}{N}} \right) e^{j\frac{2\pi\bullet 2\bullet k}{N}} \quad (13)$$

Obviously, the other terms except for $X(k)$ at the right hand side of Eq. (14) are caused by the TSE (two time shift points here). The larger the TSE, the more the number of the terms in the parenthesis at the right hand side of Eq. (13).

To investigate the influence of the TSE on the amplitude of $\tilde{X}(k)$, the absolute operation is performed on Eq. (13)

$$\left|\tilde{X}(k)\right| = \left| X(k) + (x(N+1) - x(1)) e^{-j\frac{2\pi\bullet 0\bullet k}{N}} + (x(N+2) - x(2)) e^{-j\frac{2\pi\bullet 1\bullet k}{N}} \right| \quad (14)$$

From Eq. (14), $\left|\tilde{X}(k)\right| \neq \left|X(k)\right|$. That is, the TSE introduces an error in the amplitude of the DFT of $\tilde{x}(n)$. However, when the time delay is not significant, the error will be small enough to negligible. This result is observed by analyzing Eq. (14). Here we just concern mode shapes, so the *k*th frequency point must be associated with one mode. Thus if this mode is excited properly, $\left|X(k)\right|$ will exhibit as a peak in the amplitude spectrum of DFT, and $\left|X(k)\right|$ and its real and/or imaginary parts must be very large in magnitudes compared with the other terms in the parenthesis. Therfore, the difference between $\left|\tilde{X}(k)\right|$ and $\left|X(k)\right|$ may be small enough to negligible for relatively small TSEs.

As for the influence of the TSE on the phase of the DFT of $\tilde{x}(n)$, there are two parts, one is contributed by the two terms in the parenthesis at the right side of Eq. (13), and the other is the term $e^{j\frac{2\pi\bullet 2\bullet k}{N}}$ outside the parenthesis. For the first part, let us consider the part in the parenthesis as the sum of three vectors in a complex plane. As we discussed before, the vector $X(k)$ is very large in modulus, and the other two terms are small in modulus. Therefore, the sum of the three vectors are very close to the vector with large modulus, $X(k)$, and thus the contribution on the phase error from the first part will be small enough to negligible, when the time delay is not that large. Then, Eq. (14) can be approximated as

$$\tilde{X}(k) \approx X(k) e^{j\frac{2\pi\bullet 2\bullet k}{N}} \quad (15)$$

For a general case, if the time shift between the two signals is Δn, the phase shift between their DFTs will be $\frac{2\pi\bullet\Delta n\bullet k}{N}$, which can be rearranged as

$$\frac{2\pi\bullet\Delta n\bullet k}{N} = \frac{2\pi\bullet\Delta n\bullet k}{N}\bullet\frac{\Delta f}{\Delta f} = 2\pi f_m \frac{\Delta n}{f_s} = \omega_m \delta t \quad (16)$$

where it is assumed that the *m*th natural frequency is associated with the *k*th frequency point. f_m and ω_m are the *m*th natural frequency and its circular frequency. Δf is the frequency resolution, and $\frac{\Delta n}{f_s}$ is actually the TSE δt.

Now let us get back to study the influence of the TSE on the amplitude and phase of identified mode shapes. Assuming that the TSE between the *i*th wireless sensor and the time reference sensor is δt_i. The digital response data measured from the *i*th sensor is expressed as

$$\tilde{x}_i(n) = x_i(n + \delta t_i) \quad (17)$$

Based on Eqs. (15) and (16), for the *m*th mode (associated with the *k*th frequency point), its DFT can be expressed as

$$\tilde{X}_i(k) \approx X_i(k) e^{j\omega_m \delta t_i} \quad (18)$$

Eq. (18) is consistent with Eq. (9) if we ignore the some errors caused by the TSE.

Before using the FDD method to identify mode shapes, let us rearrange the CSD matrix at the *m*th natural frequency in Eq. (1) as

$$\mathbf{G}(\omega_m) = \mathbf{G}(k) = \begin{bmatrix} X_1(k) \\ \vdots \\ X_i(k) \\ \vdots \\ X_n(k) \end{bmatrix} \begin{bmatrix} X_1^*(k) & \cdots & X_i^*(k) & \cdots & X_n^*(k) \end{bmatrix} \quad (19)$$

Just like in Eq. (19), the CSD matrix of the responses with TSEs at the *m*th natural frequency can be written as

$$\tilde{\mathbf{G}}(\omega_m) = \tilde{\mathbf{G}}(k) = \begin{bmatrix} \tilde{X}_1(k) \\ \vdots \\ \tilde{X}_i(k) \\ \vdots \\ \tilde{X}_n(k) \end{bmatrix} \begin{bmatrix} \tilde{X}_1^*(k) & \cdots & \tilde{X}_i^*(k) & \cdots & \tilde{X}_n^*(k) \end{bmatrix} \quad (20)$$

Substituting (18) into (20) and considering (19) yields

$$\tilde{\mathbf{G}}(\omega_m) \approx \mathbf{P}\mathbf{G}(\omega_m)\mathbf{P}^* \tag{21}$$

where $\mathbf{P}$ is called the time synchronization error matrix herein. $\mathbf{P}$ is a diagonal matrix and its diagonal elements are

$$diag(\mathbf{P}) = \left[e^{i\omega_m \delta t_1} \quad \cdots \quad e^{i\omega_m \delta t_i} \quad \cdots \quad e^{i\omega_m \delta t_n} \right] \tag{22}$$

To identify the *m*th mode shape from the responses with TSEs, the SVD is performed on $\tilde{\mathbf{G}}(\omega_m)$ by solving an eigenvalue problem like Eq. (2). Considering Eqs. (21) and (3), $\tilde{\mathbf{G}}(\omega_m)\tilde{\mathbf{G}}^*(\omega_m)$ can be expressed as

$$\begin{aligned} \tilde{\mathbf{G}}(\omega_m)\tilde{\mathbf{G}}^*(\omega_m) &\approx \mathbf{P}\mathbf{G}(\omega_m)\mathbf{P}^*(\mathbf{P}^*)^*\mathbf{G}^*(\omega_m)\mathbf{P}^* \\ &= \mathbf{P}\mathbf{U}\boldsymbol{\Sigma}\mathbf{P}^*\mathbf{P}\boldsymbol{\Sigma}^*\mathbf{U}^*\mathbf{P}^* \end{aligned} \tag{23}$$

Because both $\boldsymbol{\Sigma}$ and $\mathbf{P}$ are diagonal matrices, Eq. (23) can be rearranged as

$$\tilde{\mathbf{G}}(\omega_m)\tilde{\mathbf{G}}^*(\omega_m) \approx \mathbf{P}\mathbf{U}\mathbf{P}^*\boldsymbol{\Sigma}\boldsymbol{\Sigma}^*\mathbf{P}\mathbf{U}^*\mathbf{P}^* \tag{24}$$

Comparing Eq. (24) and Eq. (2), Eq. (24) is rewritten as

$$\tilde{\mathbf{G}}(\omega_m)\tilde{\mathbf{G}}^*(\omega_m) \approx \tilde{\mathbf{U}}\boldsymbol{\Sigma}\boldsymbol{\Sigma}^*\tilde{\mathbf{U}}^* \tag{25}$$

Therefore, $\tilde{\mathbf{U}}$ is the left singular decomposition matrix of $\tilde{\mathbf{G}}(\omega_m)$

$$\tilde{\mathbf{U}} \approx \mathbf{P}\mathbf{U}\mathbf{P}^* \tag{26}$$

According to the fundamental theory of the FDD method, the first column of $\tilde{\mathbf{U}}$ is an estimation of the *m*th mode shape, designated as $\tilde{\mathbf{U}}_1$. To get the normalized mode shape of $\tilde{\mathbf{U}}_1$, each component is divided by the reference component (say, the *r*th component)

$$\tilde{\mathbf{U}}_1 \approx \begin{bmatrix} \dfrac{e^{i\omega_m\delta t_1 - i\omega_m\delta t_1}\mathbf{U}_{1,1}}{e^{i\omega_m\delta t_r - i\omega_m\delta t_1}\mathbf{U}_{r,1}} \\ \vdots \\ \dfrac{e^{i\omega_m\delta t_i - i\omega_m\delta t_1}\mathbf{U}_{i,1}}{e^{i\omega_m\delta t_r - i\omega_m\delta t_1}\mathbf{U}_{r,1}} \\ \vdots \\ \dfrac{e^{i\omega_m\delta t_n - i\omega_m\delta t_1}\mathbf{U}_{n,1}}{e^{i\omega_m\delta t_r - i\omega_m\delta t_1}\mathbf{U}_{r,1}} \end{bmatrix} = \begin{bmatrix} e^{i\omega_m(\delta t_1 - \delta t_r)}\dfrac{\mathbf{U}_{1,1}}{\mathbf{U}_{r,1}} \\ \vdots \\ e^{i\omega_m(\delta t_i - \delta t_r)}\dfrac{\mathbf{U}_{i,1}}{\mathbf{U}_{r,1}} \\ \vdots \\ e^{i\omega_m(\delta t_n - \delta t_r)}\dfrac{\mathbf{U}_{n,1}}{\mathbf{U}_{r,1}} \end{bmatrix} \tag{27}$$

where $\tilde{\mathbf{U}}_1$ denotes the mode shape identified from the data with TSEs, and $\mathbf{U}_{i,1}$ denotes the *i*th mode shape component identified from the data without TSEs. δt_r is the TSE of response at the reference point (or *r*th component).

It is clear that the TSE affect both the amplitudes and phases of the mode shape components. However, if the TSE is relatively small, the amplitude errors and partial of phase errors of the DFTs of the responses will be small enough to be negligible, and accordingly, so will be the ampitude error and partial phase error of the mode shapes.

However, the other phase errors cannot be ignored. As shown in Eq. (27), for the *i*th component, the phase shift between them is equal to $\omega_m(\delta t_i - \delta t_r)$, which is a consequence of the presence of TSEs between wireless sensors. For the same TSE, the higher the order of the mode, the greater the natural frequency ω_m, and the greater the phase shift.

If the phase shift of one component in the normalized $\tilde{\mathbf{U}}_1$ is great enough to force the phase of this component into another region, for instance, from $[-\pi/2 \quad \pi/2]$ to $[\pi/2 \quad 3\pi/2]$, the sign of this mode shape component will be changed, and the identified mode shape will be severely distorted.

Because it is difficult to estimate TSEs between wireless sensors, one cannot easily obtain information on the phase shifts of mode shape components and thus cannot completely adjust the signs of the distorted mode shapes. But if one neglects phase information and assumes all the mode shape components have the same sign, one can use modified values of the mode shapes by only keeping information on the magnitudes of mode shape components. Actually, these modified mode shapes are the absolute values of distorted mode shapes, called here Absolute Mode Shape (AMS). The distortion of identified mode shapes caused by TSEs and the capability of this approximation strategy will be illustrated in Fig. 3 by an example of a simply supported beam. This strategy is simple, but very useful when paired with an appropriate damage detection technique. It makes damage detection based on a WSN with large TSEs still effective, and thus extends the time resynchronization period of a WSN.

IV. Damage detection strategies based on the distorted mode shapes and the AMSs

When the TSE is relatively small, the amplitude errors in the mode shapes caused by the TSE can be negligible. Under this condition, there are two ways to implement detect damage methods when the identified results of mode shapes are distorted by non-synchronized sensing in WSNs. One is to directly employ the distorted mode shapes, thus a damage detection method which still works with them will be identified. The other is to apply the modified mode shapes (the AMS) to damage detection.

A. Damage detection strategies using distorted modes

Although mode shapes may be distorted by TSEs between wireless sensors, recognizing that only the signs of some mode shape components are changed, the classical flexibility difference method is still applicable with distorted mode shapes, as illustrated below.

From (5), it is observed that the diagonal element in the classical flexibility matrix is the square sum of *n* terms. Note that if the magnitudes of mode shape magnitudes remain unchanged, even if their signs are incorrect, the diagonal elements of the constructed **F** from these mode shapes will be equal to the real ones. In the presence of TSEs between wireless sensors, if the distorted mode shapes are used, although the signs of some mode shape components are not correct, the diagonal elements of **F** will not be affected, in theory. Therefore, the damage indicators extracted from the diagonal entries of flexibility are still effective when the distorted mode shapes are used to assemble flexibilities. Here, the percentage changes in diagonal entries of flexibilities before and after damage are taken as the damage indicators.

B. Damage detection based on the AMSs

Because the classical flexibility difference method works for the distorted mode shapes, it must work with the AMSs. However, the method itself cannot localize damage to the exact members. To achieve this goal, the ASHF method is employed. Here AMSs are used to construct the ASH flexibility by Eq. (6), and the damage indicators are extracted from the difference in the ASH flexibilities before and after damage. The feasibility of applying AMSs to the ASHF method is analyzed:

1) Due to the sign adjustment in finding the AMS, the magnitudes of the ASH mode shape components calculated from the AMSs are equal to those calculated from the real mode shapes, except for the ASH mode shape components corresponding to the elements near the nodes of the modes, which will introduce some errors to the constructed ASH flexibility, as shown in the schematic diagram of the AMSs of a simply supported beam (Fig. 1). The higher the mode order, the more nodes there are, and the greater the effect on the ASH mode shape components. Fortunately, the higher the mode order, the smaller the contribution of the ASH mode shape to the ASH flexibility; on the other hand, the mode shape components near the nodes are small in magnitude.

2) Although the signs of some components in ASH mode shapes calculated from the AMSs are not correct compared with the real ASH mode shapes, it is the same case for both intact and damaged states. Therefore, the ASH flexibility-based method still works when the AMSs are available.

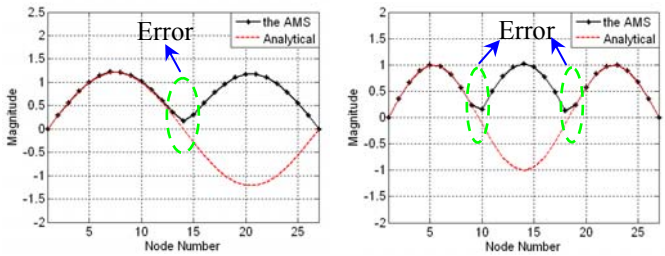

a) the 2nd AMS after the adjustment b) the 3rd AMS after theadjustment

Fig. 1 Schematic diagram of comparison between the AMS and real mode shape

V. NUMERICAL SIMULATIONS

To validate the performance of the proposed strategies, a simply supported beam is first studied. The beam is assumed to be made of aluminum with dimensions 2080mm×20mm×20mm. The Young's modulus and mass density of the material are 70GPa and 2700kg/m^3, respectively. It is modeled using 26 beam elements, each of 80mm long, as shown in Fig. 2, with 27 nodes and two DOFs at each node. The first five analytical natural frequencies are 10.67, 42.59, 95.54, 169.13 and 262.84 Hz.

Assume that viscous dissipation is included in the form of orthogonal damping with a magnitude of 1% of critical in each mode of the structure. A band-limited, random white noise is applied at all nodes to simulate ambient vibration. Simulated acceleration responses in the vertical direction are computed by Newmark-Beta integration. It is assumed that the sampling rate is 1152 Hz. The noise of the response at each node is prescribed to have an RMS equal to 5% of that of the corresponding response.

A. Influence of TSEs on identified mode shapes

The intact structure is considered here. The TSEs between wireless sensors are simulated with time delays between responses. The time delay vector is generated randomly, and the maximum value is 50/1152 sec (50 time steps). The time delays at all nodes are 44, 29, 42, 21, 17, 0, 9, 8, 6, 36, 48, 50, 30, 29, 16, 49, 5, 36, 27, 20, 10, 35 and 2 time steps.

Fig. 2 FEM of the simply supported beam

The FDD method is employed to identify modal parameters. The first five mode shapes are identified from the data with time delays and the first two representative mode shapes are plotted in Fig. 3. The solid line represents the identified mode shape, and the dashed line is the analytical mode shape. Clearly, the identified mode shapes are severely distorted. Only some components in the identified mode shapes agree with the analytical ones. Those components that deviate from the corresponding analytical ones have nearly the same magnitudes as the analytical ones, with an opposite sign. These results are consistent with the theoretical analysis in Section III. Note that the amplitude errors are very small.

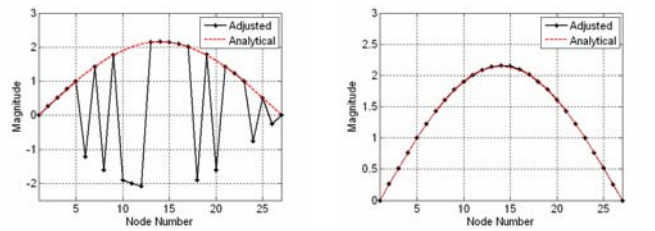

(a) the 1st identified mode shapes without adjustment (b) the 1st AMS after the adjustment

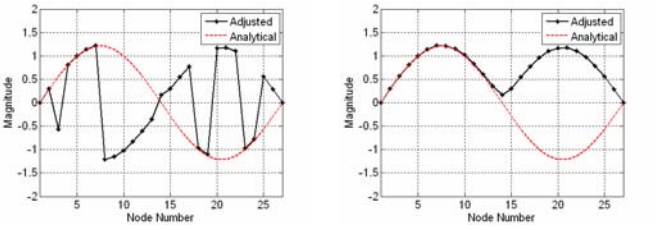

(c) the 2nd identified mode shapes without adjustment (d) the 2nd AMS after the adjustment

Fig. 3 The influence of the lack of time synchronization on the identification results of mode shapes and the corrected mode shapes

Using the proposed correction strategy in Section III, the AMSs are obtained and they are also presented in Fig. 3. For the first order, the AMS agrees with the analytical one, which means the distorted mode shape is appropriate user. For the higher orders, the distorted mode shapes are modified to some extent.

B. Damage localization using distorted modes and AMSs

Both the ASH flexibility-based method and the classical flexibility difference method are employed to localize damage in the simply supported beam.

The damage is simulated as 50% reduction of Young's moduli in elements 4 and 22. Three cases with different time delays are studied with the maximum time delays 10/1152, 20/1152 and 50/1152 sec, respectively. To demonstrate the robustness of the proposed strategies in practice, different time delay vectors are randomly generated by using different seeds for intact and damage states in each case.

The procedures for locating damage using the ASHF method are as follows. First, the distorted mode shapes are modified to obtain the AMSs. Then, the ASH flexibility is constructed using AMSs and natural frequencies. Third, the maximum absolute values of elements in each column of the difference between ASH flexibility matrices before and after damage are extracted as damage indicators.

Different numbers of modes are used to assemble the ASH flexibility. Only the results using the first five modes are listed here. The damage localization results with the ASHF method are presented in Figs. 5-7. When the maximum time delays are 10/1152 sec and 20/1152 sec, the results suggest that the ASH flexibility-based method can easily localize the damage to the exact elements by observing "step and jump" in the plot of "Element Number" vs. "Change in ASHF". When the time delay is 50/1152 sec, although the damage localization results are not as good as the other two cases, they still could provide an indication of damage sites. However, if the proposed strategy is not used, the ASHF method with the AMS fails to localize the damage even when the maximum time delay is 5/1152 sec. Therefore, the damage detection strategy is able to be tolerant of TSEs, and the TSE tolerance is 50/1152 sec.

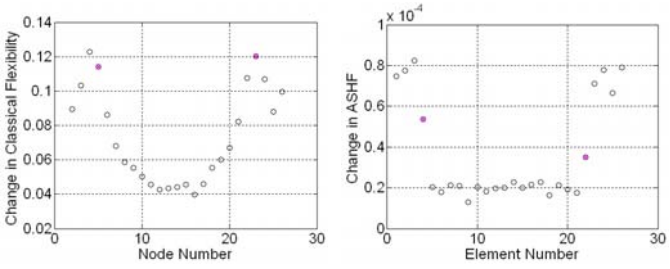

(a) the classical flexi. based method (b) the ASH flexi. based method

Fig. 5 The results when using the maximum time delay of 10/1152 sec

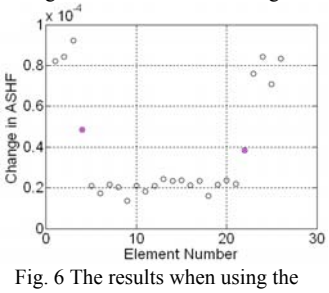

Fig. 6 The results when using the maximum time delay of 20/1152 sec

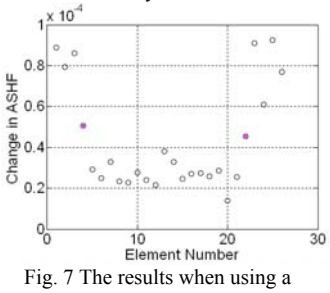

Fig. 7 The results when using a maximum time delay of 50/1152 sec

The damage location results using the classical flexibility difference method for each case are also presented in Fig. 5 for comparison. Although there are peaks around the two damage sites, it is difficult to determine the exact damage elements. To directly localize damage to the exact element is one advantage of the ASHF method over the classical flexibility difference method.

VI. Conclusions

Damage localization strategies based on WSNs with the capability of being tolerant of large time synchronization errors are proposed, when the amplitude errors of the identified mode shapes caused by the TSE can be negligible. The authors show how TSEs in the WSN distorts the identification results of mode shapes, and presented two possible solutions. First, a damage detection method is identified which works with the distorted mode shapes. Second, a strategy for using modified versions of the distorted mode shapes is developed based on the system identification results without time synchronization between wireless sensors. Then the modified mode shapes are applied in the ASHF method to localize damage to the exact elements. Numerical simulation results of a simply supported beam demonstrate that the aforementioned proposed strategies relax the requirement of frequent sensor synchronization, without sacrificing accuracy in damage localization.

Acknowledgment

The first author would like to acknowledge support of the National Natural Science Foundation of China under Grant No. 50708029.

References

[1] M. A. Horton, S. Glaser, and N. Sitar, "Wireless networks for structural health monitoring and hazard mitigation", *Proc. of the US-Europe Workshop on Sensors and Smart Structures Technology*, 2002, pp. 19-23.

[2] J. P.Lynch, A. S. Kiremidjian, K. H. Law, T. Kenny and E. Carryer, "Issues in wireless structural damage monitoring technologies", *Proc. of the Third World Conference on Structural Control*, 2002, Vol.2, pp. 667-672

[3] Spencer, B.F., "Opportunities and challenges for smart sensing technology". *First International Conference on Structural Health Monitoring and Intelligent Infrastructure*, Tokyo, November 2003.

[4] Romer, K., "Time synchronization in Ad Hoc Networks", *Proc. of the 2nd ACM symposium on Mobile Ad Hoc networking and computing*, Long Beach, California, 2001, pp. 173-182.

[5] J. Elson, L. Cirod, and D. Estrin, "Fine-grained network time synchronization using reference broadcasts", *Proc. of the 5th symposium on operating systems design and implementation*, Boston, 2002.

[6] M. Maroti, B. Busy and G. Simon et al., "The flooding time synchronization protocol", *Proc. Of the 2nd CAN Cof. on embedded networked sensor systems*, Baltimore, Maryland, 2004, pp. 39-49.

[7] Tomonori Nagayama, "Structural health monitoring using smart sensors", Ph.D. Dissertation. University of Illinois at Urbana-Champaign, 2007

[8] V Krishnamurthy, K Fowler and E Sazonov. The effect of time synchronization of wireless sensors on the modal analysis of structures, Smart Materials and Structures, 17 (2008): 1-13

[9] R. Brinker, L.M. Zhang, P. Andersen, "Modal identification from ambient responses using frequency domain decomposition", *Proceedings of the 18th IMAC*, San Antonio, TX, 2000, pp. 625-630.

[10] G. Kerschen and J.C. Golinval. Physical Interpresentation of the Proper Orthogonal Modes Using the Singular Value Decomposition. Journal of Sound and Vibration 2002, 249(5): 849-865.

[11] Pandey AK, Biswas M., Experimental Verification of Flexibility Difference Method for Locating Damage in Structures. Journal of Sound and Vibration 1995, (184): 311-328

[12] Zhongdong Duan, Guirong Yan and Jinping Ou, "Structural Damage Detection Using the Angle-between-String-and-Horizon Flexibility", Submitted to Journal of Sound and Vibration and under review.